Hybrid RANS-LES Models

Koen Geurts[1] and Axel Probst[2]

[1] Institute of Aerodynamics, RWTH Aachen University
[2] Institute of Aerodynamics and Flow Technology, DLR Göttingen

Abstract. A fully coupled zonal Reynolds-averaged Navier-Stokes (RANS) – large-eddy simulation (LES) method and a hybrid Detached-Eddy Simmulation (DES) method are presented and results for a subsonic flow over the HGR-01 airfoil at high angle of attack are discussed for both methods. Attached boundary layers are computed by RANS and separated flow regions are determined by LES methods, resulting in a higher accuracy solution with respect to pure RANS solutions, at a lower cost than a pure LES computation.

1 Introduction

The numerical analysis of flow fields in industrial applications is nowadays mainly based on solutions of the Reynolds-averaged Navier-Stokes equations (RANS). When unsteady flow phenomena such as a local separation, are to be investigated or a physical problem is dominated by vortical structures with time or length scales but only in the range of the inertial subrange the approach based on standard Reynolds-averaged Navier-Stokes equations is often not the appropriate choice to describe the flow field. This is, for instance, the case when the flow over a flap-airfoil configuration is considered, as done by Zhang [17], or when a separation region exists due to a transonic shock-boundary-layer interaction [11]. It is therefore desired to investigate more accurate RANS formulations or combine LES and RANS simulation methods.

In the present paper, a Detached-Eddy Simulation (more specifically an AD-DES model) and a fully coupled zonal RANS-LES method are applied to the unsteady flow around the subsonic research profile HGR-01 which features a mixed stall behaviour where a laminar separation bubble (LSB) and trailing edge separation (TES) occur at high angles of attack.

The paper starts with a description of the applied numerical methods and the computational set-up for the different computations. The results of the AD-DES model and the zonal RANS-LES model are compared to a pure RANS computation, with a Reynolds Stress Model (RSM) pure LES computation and experimental data. The unsteady flow phenomena and the time-averaged airfoil characteristics are discussed before concluding remarks of the findings are given.

N. Kroll et al. (eds.), *Computational Flight Testing*, Notes on Numerical Fluid Mechanics and Multidisciplinary Design 123,
DOI: 10.1007/978-3-642-38877-4_3,

2 Numerical Methods

2.1 Large-Eddy Simulation

A pure large-eddy simulation (LES) computation is performed as a validation for the experimental data and as reference for the ADDES and the zonal RANS-LES computation. The three-dimensional unsteady compressible Navier-Stokes equations are solved based on a large-eddy simulation using the MILES (monotone integrated LES) approach[1]. The vertex-centered finite-volume flow solver is block-structured. A modified AUSM method is used for the Euler terms [6], which are discretized to second-order accuracy by an upwind-biased approximation. For the non-Euler terms a centered approximation of second-order is used. The temporal integration from time level n to $n+1$ is done by a second-order accurate explicit 5-stage Runge-Kutta method, the coefficients of which are optimized for maximum stability. For a detailed description of the flow solver the reader is referred to Meinke *et al.* [7].

2.2 Detached-Eddy Simulation

The detached-eddy simulation (DES) [14] is a non-zonal hybrid RANS-LES method, in which a conventional RANS turbulence model is enabled to act as a subgrid-scale LES model in massively separated (i.e. detached) flow regions. In original DES the switching between RANS and LES mode is based on a comparison of the RANS length scale l_{RANS} and a calibrated LES scale l_{LES}, which depends on the local grid spacing $\Delta_{DES} = \max(\Delta_x, \Delta_y, \Delta_z)$. Later extensions were aimed to "shield" attached boundary layers from premature switching to LES mode (Delayed DES, *DDES*) and to extend the method by wall-modelled LES capabilities e.g. in reattached flows (Improved DDES, *IDDES*). However, according to earlier studies on the HGR-01 airfoil [16], these classic DES variants may either strongly overestimate the trailing-edge separation due to modelled-stress depletion, or retain the whole separation in RANS mode. In that case, no improvement over the much cheaper RANS approach is obtained.

Algebraic Delayed Detached-Eddy Simulation. In order to broaden the range of applicability of DES to incipient stall cases, the basic DDES was extended by algebraic relations for the so-called "delay function". It is designed to reliably shield attached boundary layers from LES mode and to detect separation onset for a proper placement of the RANS-LES interface. This Algebraic DDES (ADDES) [10] was implemented in the DLR-TAU code and tested for the HGR-01 flow in combination with the Spalart-Allmaras one-equation model and the JHh-RSM. The SST-ADDES computations are performed with the finite-volume code DLR-TAU [13], which solves the compressible flow equations on unstructured meshes. The spacial discretization for convection applies a second-order central scheme in skew-symmetric form which is stabilized by matrix-weighted artificial dissipation with low-Mach-number preconditioning. Time integration is based on second-order dual-timestepping with an implicit LU-SGS scheme for the inner pseudo timesteps.

2.3 Zonal RANS-LES

The zonal RANS-LES computation uses separate and overlapping RANS and LES domains. The LES domains are chosen to be as small as possible to reduce the number of grid points required without decreasing the local accuracy. Due to the small LES domains, the LES inflow boundaries are subject to large pressure gradients. At the overlapping in- and outflow boundaries, a sponge/forcing layer is applied to realise a smooth transition between RANS and LES and visa versa. To also ensure a smooth transition from the three-dimensional unsteady LES solution to the two-dimensional RANS solution, another sponge/forcing layer is applied to damp high frequency pressure and velocity fluctuations at the overlapping region from the LES domain to the RANS domain. Further details of such a sponge layer can be found in Zhang *et al.* [17] .

LES-to-RANS Boundary. When going from an LES to a RANS domain, a relevant value for the eddy viscosity is required at the inflow boundary of the RANS domain. This value is reconstructed at the inflow plane using the $k-\omega$ turbulence model [5] . The quantity ω is computed from the normal components of the Reynolds stress tensor using Bradshaw's hypothesis. The turbulent kinetic energy k is determined from the transport equation.

RANS-to-LES Boundary. At the inflow of the LES domains, the turbulent boundary layer is reproduced using synthetic turbulence. The synthetic turbulence generation method of Jarrin *et al.* [3] is based on a superposition of coherent structures. Applications of the synthetic-eddy method (SEM) often suffer from a long transition length until a physically correct fully developed turbulent boundary layer is obtained. Therefore, the idea of Keating [9] to apply controlled forcing [15] to shorten this turbulence development region downstream of the LES inflow boundary is applied. The local control planes of Spille and Kaltenbach [15] introduce a volume forcing term to the Navier-Stokes equations to control the turbulence production in the boundary layer and reduce the required overlapping length of the different computational domains. This zonal RANS-LES method was successfully validated by Roidl *et al.* [12,11] .

Time Averaging. For a proper averaging of the large scale structures due to the unsteady behavior of the TES, the zonal computation as well as the pure LES computation require data samples of about 2 c/U_∞ for the velocity profiles and 5 c/U_∞ for smooth pressure and skin-friction distributions and velocity profiles.

3 Computational Set-Up

3.1 HGR-01 Airfoil

The near stall flow phenomena of the HGR-01 research airfoil were studied at several angles of attack [16] . In this study, the configuration at an angle of

attack of 12^o with a laminar separation bubble and trailing-edge separation is simulated at a Reynolds number of $Re_c = 0.65 \cdot 10^6$ based on the chord length c. The high angle of attack flow over the HGR-01 profile is a demanding test case for numerical simulations, since the flow field exhibits a small laminar separation bubble with laminar-to-turbulent transition at the leading edge, a critical positive pressure gradient on the upper surface and a trailing-edge separation at about 90% chord length.

3.2 Computational Meshes

Pure LES. The grid resolution for the pure LES computation is chosen according to Zhang *et al.* [17]. The resolution of the pure LES grid in the streamwise, wall normal, and spanwise direction of $\Delta x^+ \approx 100$, $\Delta y^+_{min} \approx 1$ and $\Delta z^+ \approx 20$. The grid is build up out of 32 structured blocks in a C-grid configuration around the airfoil and can be seen in Fig. 1(a). The grid extends 4 chord lengths in spanwise direction, using periodic boundary conditions at these boundaries. The farfield boundaries are located further than 20 chord lengths from the HGR-01 profile to mimic free stream conditions. This results in a total number of grid points of 51.4 million.

Detached-Eddy Simulation. In detached-eddy simulations, the grid resolution is mainly governed by the separated regions treated in LES mode, which should be highly resolved by mostly isotropic cells. Thus, a hybrid C-type mesh with 460×92 grid points on the airfoil is used, which is specifically refined in the upper trailing-edge and wake region. The local streamwise grid spacing of $\Delta x/c \approx 0.23\%$ roughly corresponds to the spanwise spacing of $\Delta z/c \approx 0.234\%$, which results from $n_z = 64$ layers within the spanwise extent of $L_z = 0.15c$. As the attached 2D-flow regions in RANS mode theoretically require no 3D resolution, an optional spanwise grid adapation confined to the trailing-edge region is considered. Besides the fully 3D-resolved grid ("base grid", 4.9 million points), two adapted meshes with a transition at $x/c \approx 0.5$ from 1 to 64 ("$n_z = 1 \rightarrow 64$", 2.8 million points) and 2 to 128 ("$n_z = 2 \rightarrow 128$", 5.5 million points) spanwise layers, respectively, are generated for an assessment of grid sensitivities. The temporal discretization is estimated from the requirement of a convective CFL number well below 2/3 in the LES region. This yields a basic timestep of $\Delta t = 0.001 c/U_\infty$.

Zonal RANS-LES The grid resolution for the LES domain of the zonal RANS-LES simulation is equal to the pure LES computation. The RANS domains use a coarser grid in all directions, however, $\Delta y^+_{min} \approx 1$ is still maintained at the airfoil surface. This results in a total of $13.2 \cdot 10^6$ grid points divided over the LES and RANS domains. This corresponds to a reduction of grid points by a factor of four with respect to the pure LES computation.

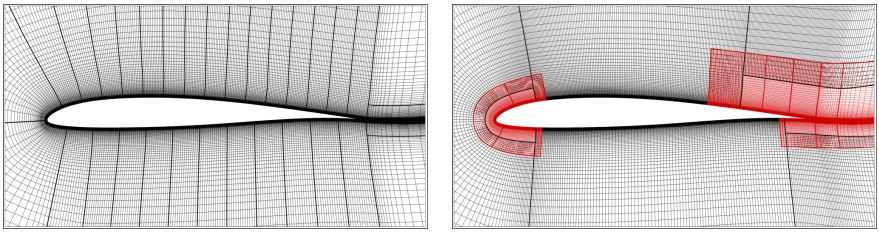

(a) LES grid (b) Zonal grid

Fig. 1. Computational grids (for the zonal grid: red/fine = LES, black/coarse = RANS)

4 Results

4.1 Zonal RANS-LES Results

Fig. 2 shows the averaged pressure coefficient c_p of the different computations in comparison to the experimental data. The grey shaded areas represent the embedded LES domains around the leading and trailing edge for the zonal RANS-LES computation.

The pure LES results agree well with the experimental data on the upper and lower surface, validating the precision of the LES computation and confirming the quality of the wind tunnel measurements. The LSB and the TES are reproduced, however the size of the LSB is underestimated slightly with respect to the experimental data.

The zonal RANS-LES results show a smooth transition from the LES to the RANS, and the RANS to the LES zone. The suction peak with the laminar separation bubble evidenced by the experimental data is nicely reproduced by the LES region.

When comparing the zonal RANS-LES results of the skin-friction coefficient to the pure LES computation in Fig. 3, it can be seen again that the zonal method accurately reproduces the leading edge flow with the LSB. The pure RANS computation with the RSM model uses a fixed transition point and underpredict the size of the LSB. Concerning the TES, the RANS and LES based methods predict separation, however, both the zonal RANS-LES and pure RANS computation result in a slightly smaller recirculation area.

A more detailed analysis of the boundary layer velocity profiles at the upper surface of the airfoil in Fig. 4. These velocity profiles are located at several streamwise positions on the upper surface of the HGR-01 airfoil in the embedded LES domains. The profiles from left to right represent the LSB at $0.012\,c$, the velocity profile just upstream of the RANS inflow boundary at $0.12\,c$, and three profiles in the trailing edge LES region, i.e. at $0.68\,c$, $0.85\,c$, and $0.95\,c$.

At the leading edge, the zonal computation accurately reproduces the pure LES velocity profiles. The size of the LSB is slightly underpredicted by the zonal method. Note that the velocity profile at $0.12\,c$ is the profile that is transferred to the RANS inlet boundary. It coincides with the pure LES velocity profile,

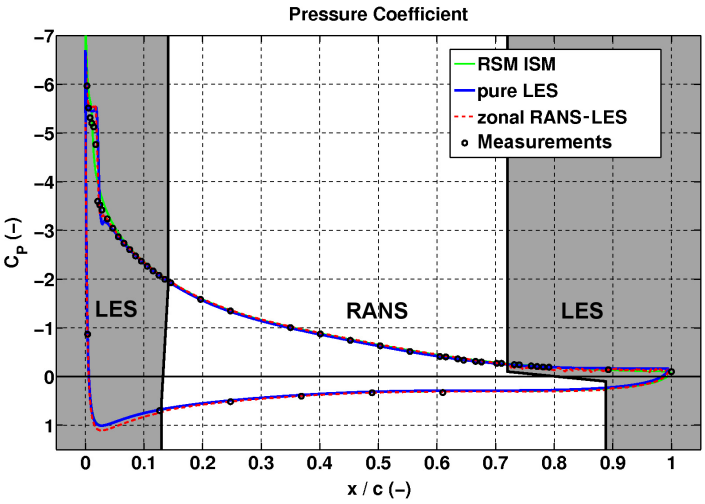

Fig. 2. Pressure coefficient c_p at the upper and lower surface of the HGR-01 airfoil for the ϵ_h, the zonal RANS-LES, pure LES computations, and experiments [16]

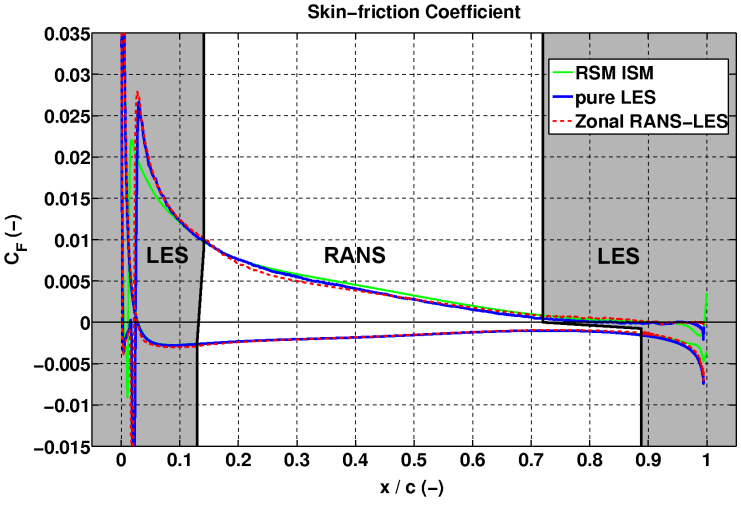

Fig. 3. Skin-friction coefficient c_f at the upper and lower surface of the HGR-01 airfoil for the ϵ_h, the zonal RANS-LES, pure LES computations

showing the accurate simulation of the leading edge flow, the LSB, and the laminar-to-turbulent transition.

At the trailing-edge separation region, the results of the averaged zonal RANS-LES and the pure LES are compared with particle-image velocimetry (PIV) data [16] to validate the numerical results. The PIV results depend on the spanwise position and show a small three-dimensional effect in the TES. The maximum span s of the experimentally investigated airfoil is 3.25 s/c and the visualized PIV results represent the velocity profiles at 1.6, 1.9, and 2.6 s/c, respectively. The pure LES computation shows very good agreement with the PIV measurements. Looking closely at the velocity profiles at the trailing edge, it should be noted that the zonal velocity profiles deviate somewhat from the reference LES computation. They are fuller near the surface and the boundary-layer thickness is smaller. This difference, however, does not have a significant influence on the pressure and friction coefficient. From the velocity profiles it can be seen that the deviation already exists at 0.68 c.

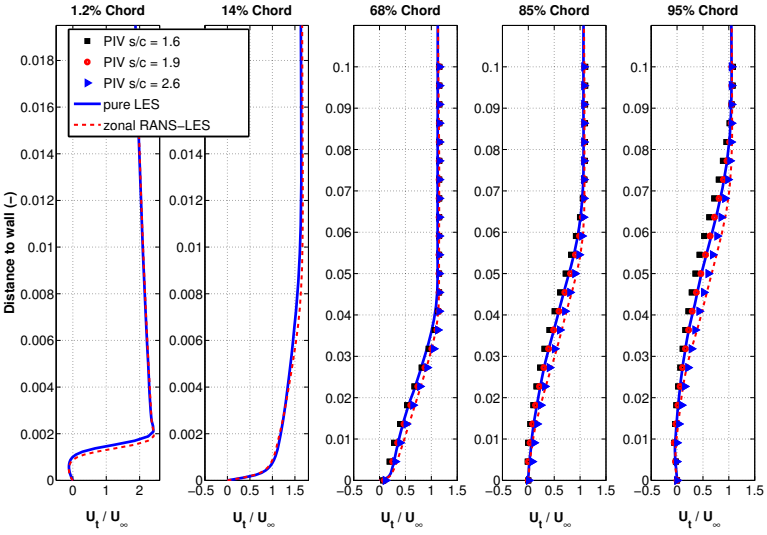

Fig. 4. Velocity profiles at the upper surface of the HGR-01 airfoil for the ϵ_h, the zonal RANS-LES, pure LES computations, and experiments [16]

Looking more closely to the velocity profiles and Reynolds stress tensor profiles somewhat downstream of the LSB at $0.045c$ in Fig. 5 and $0.12c$ in Fig. 6 it can be seen how this bubble height influences the RMS values of the velocities. Their profiles, which are scaled by the boundary layer thickness δ_0, show a smaller turbulence intensity than the pure LES. The difference in intensity for u_{RMS} and v_{RMS} decreases further downstream. The time averaged velocity and Reynolds shear stress $< u'v' >$ profiles are not influenced by the difference in height of the LSB.

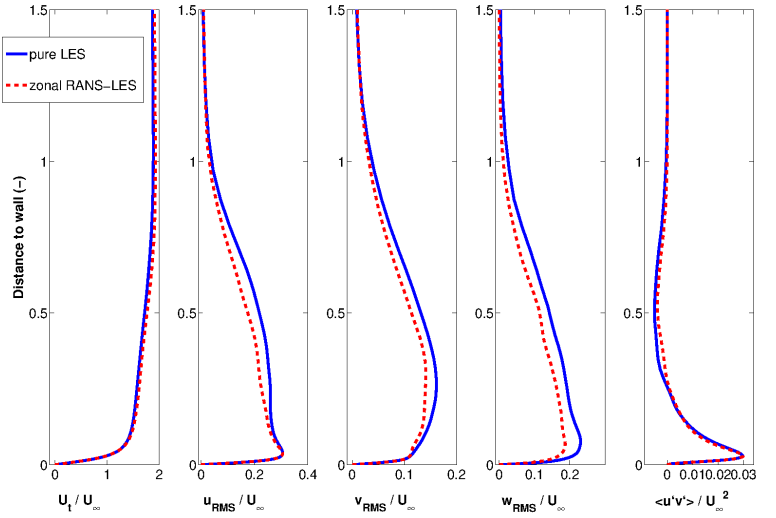

Fig. 5. Velocity and Reynolds stress tensor component profiles at $c/L = 0.045$

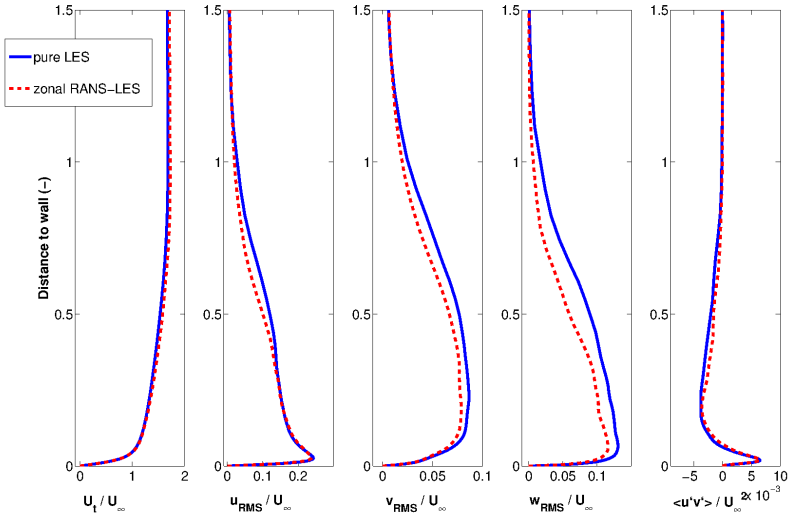

Fig. 6. Velocity and Reynolds stress tensor component profiles at $c/L = 0.12$

The velocity profiles and Reynolds shear stress in the RANS domain on the upper surface are shown in Fig. 7. The results at a streamwise position of $0.30\,c$ show only a slight deviation from the pure LES data. The Reynolds shear stress profile in the RANS domain of the zonal computation is reconstructed from the turbulent viscosity. The RANS model simulates an equilibrium boundary layer as opposed to the non-equilibrium state of the pure LES boundary layer. The equilibrium state of the RANS introduces a higher turbulence intensity, in contrast to the higher turbulence energy for the pure LES at $0.12\,c$. This results in an increasing deviation between the pure LES and the zonal RANS results. The velocity profile becomes fuller further downstream at $0.60\,c$, changing the flow characteristics at the suction side of the HGR-01 profile. This is crucial for the inflow boundary conditions of the trailing edge LES region. This effect on the RANS velocity profile was already discussed by Celic and Hirschel [2] .

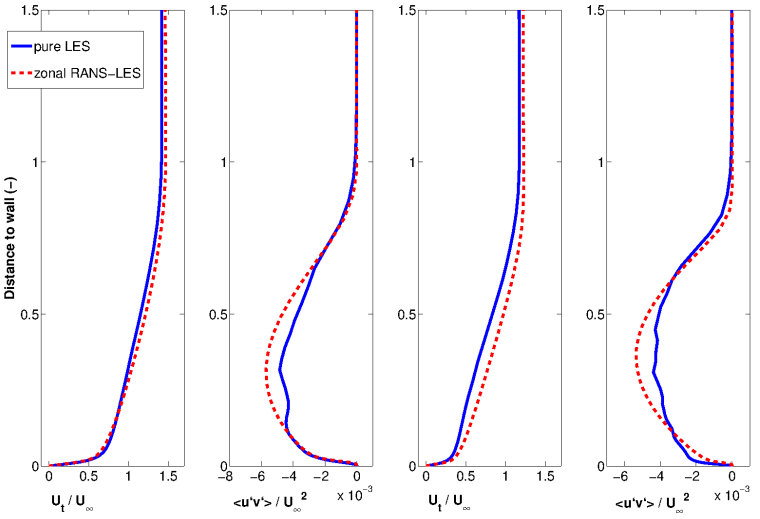

Fig. 7. Velocity and Reynolds shear stress profiles at $c/L = 0.30$ (left) and $c/L = 0.60$ (right)

Fig. 8 shows the influence of the deviating RANS velocity profile on the LES results at the trailing edge. The pure LES velocity profile and the PIV data show the separation onset at about $0.85\,c$. However, the zonal LES shows a positive velocity gradient which decreases the tendancy of the flow to separate. This results in a smaller separation region at the trailing edge for the zonal RANS-LES computation. However, as shown before, this deviation has only a limited effect on the pressure and friction coefficient distribution.

The significance of this test case is defined by the correct simulation of the LSB together with the laminar-to-turbulent transition plus the trailing-edge separation, since these phenomena influence the flow field around the airfoil and

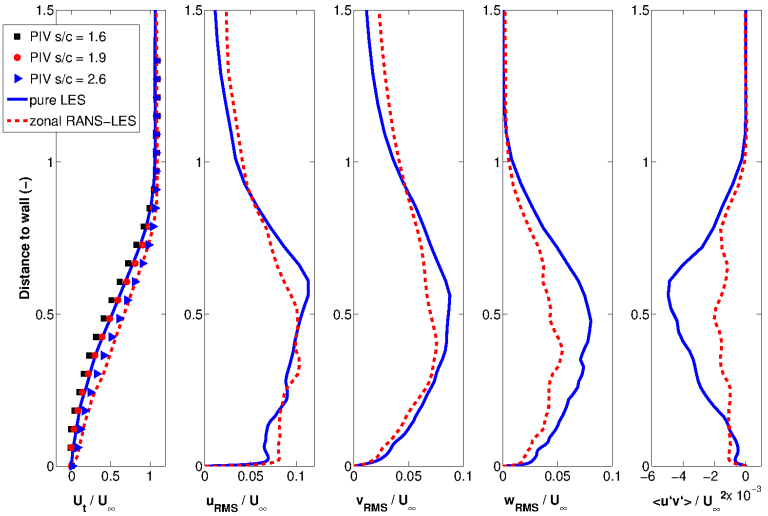

Fig. 8. Velocity and Reynolds stress tensor component profiles $c/L = 0.85$

thus the airfoil characteristics such as the lift and drag coefficients. The smaller trailing-edge separation increases the lift coefficient slightly with respect to the pure LES reference computation as shown in Table 1.

Table 1. Lift and drag coefficients of the HGR-01 airfoil for the zonal RANS-LES, pure LES computations, and experiments [16]

	Experiments	LES	Zonal RANS-LES	RANS [16]
Lift C_l	1.370	1.366	1.426	1.530
Drag C_d	0.032	0.0403	0.0414	0.028

The comparison of the characteristic values of the pure LES computation, the experiments, and the RANS data [16] shows that the zonal RANS-LES method delivers more accurate results than the RANS. The lower drag coefficient for the RANS can be explained by the almost non-existing trailing-edge separation. The RANS overestimates the lift and underestimates the drag due to the fact that the RANS model predicts the turbulent separation point too close to the trailing edge. The accuracy of the zonal computation compared to the LES reference data is determined by the limitations of the RANS model at the suction side of the profile.

4.2 ADDES Results at Increased AOA

From the SST-ADDES computation, it was observed, that the ability of the basic RANS model to capture the boundary-layer development under adverse pressure

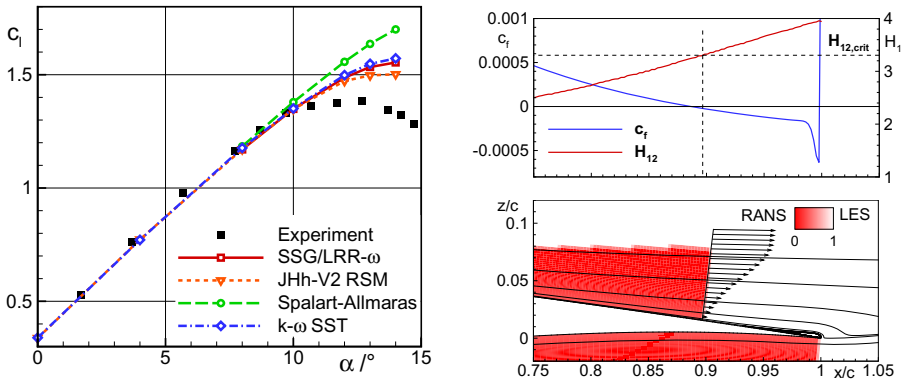

Fig. 9. *Left:* Lift-over-α curves of the HGR-01 airfoil at $Re = 0.65 \cdot 10^6$ from different RANS models and experiments [16]. *Right:* Skin friction and shape factor computed with k-ω SST (top) and resulting ADDES delay function (bottom) at the trailing edge of the HGR-01 airfoil at $\alpha = 13°$, $Re = 0.65 \cdot 10^6$.

gradients up to the separation point plays a significant role on the potentials of ADDES for airfoil stall.

The present study uses a recent combination of ADDES with the Menter SST two-equation model [8], which is considered a reasonable compromise between accuracy in the maximum-lift regime, see Fig. 9(a), and industrial requirements. The separation detector in ADDES, which is based on the shape factor H_{12}, is adjusted to the underlying RANS model and was found to match separation onset with the SST model for $H_{12,crit} = 3.3$. Figure 9(b) shows the resulting RANS/LES regions around the trailing-edge based on ADDES for the HGR-01 flow at $\alpha = 13°$. Both the full height of the attached boundary layer and the separation point at $x/c \approx 0.9$ are well captured.

Optionally, the SST-ADDES is combined with stochastic forcing for the subgrid-scale viscosity in the LES region, similar to the proposal of [4]. The method is aimed to induce small velocity disturbances, which may be amplified in the separated region and thus enhance transition from modelled to resolved turbulence. Such approaches are much easier to implement than the synthetic turbulence method used for zonal RANS/LES (see Chap. 2.3), but they only produce uncorrelated small-scale fluctuations unlike real turbulence.

Since the underlying SST-RANS model only yields only minimal trailing-edge separation at $\alpha = 12°$, the angle of attack is increased to $\alpha = 13°$ for a meaningful study of SST-ADDES. Although no detailed PIV flowfield measurements are available at this angle, the performance and the sensitivities of ADDES for incipient airfoil stall can still be assessed.

Figure 10 shows the pressure and skin-friction distributions in the airfoil's rear from the different SST-ADDES computations. As reference, the SST-RANS results and experiments (where available) are depicted. For all ADDES computations, a significant increase of the pressure plateau compared to RANS is

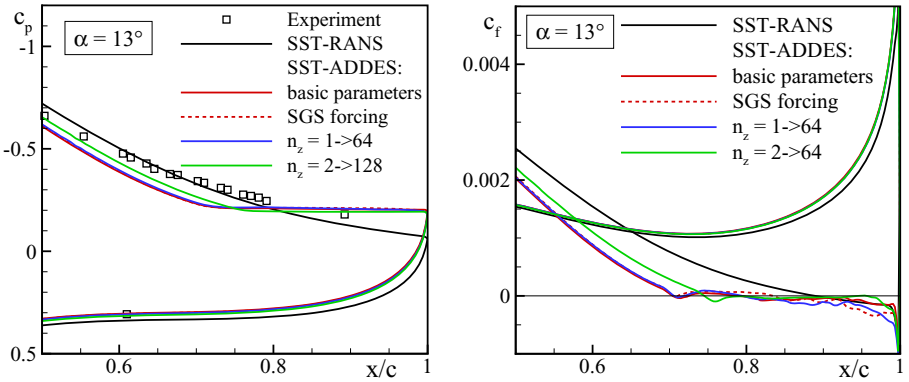

(a) Static pressure. (b) Skin-friction.

Fig. 10. Static pressure and skin-friction distributions on the HGR-01 airfoil computed with ADDES at $\alpha = 13°$

observed, which is due to an upstream shift of separation onset by almost 20 % of chord. Although the experiment features a considerable pressure plateau as well, the ADDES underestimate the upstream pressure level on the upper surface. This indicates a too large impact of the trailing-edge separation on the global airfoil circulation. Surprisingly, only the ADDES with spanwise grid refinement ("$n_z = 2 \rightarrow 128$") deviates visibly from the other simulations and yields a slightly later separation onset and reduced pressure plateau closer to measurements. For a better understanding of the flow physics, consider the visualizations of instantaneous vortical structures (Q-criterion) as well as the sum of modelled and resolved turbulent shear stress in the symmetry plane in Fig. 11. Starting with the solution of the fully-3D mesh and standard numerical settings ("basic parameters", i.e. no forcing, dissipation coefficient $k^{(4)} = 1/128$), significant turbulent content is only observed in the wake, whereas large parts of the separated region on the airfoil are free from vortical structures. Accordingly, the switch from RANS to LES mode near the separation line is clearly visible in the Reynolds stresses, as the reduction of modelled stresses to their subgrid level is not compensated by corresponding resolved stresses. Instead, a large gap with reduced total stress ("gray area") emerges, which increases the separation region beyond its physical size. A parameter variation with respect to the physical modelling ("SGS forcing") and the numerical discretization ("$n_z = 2 \rightarrow 128$") has only little effect on this behaviour. While the lowered artificial dissipation in the central scheme, $k^{(4)} = 1/160$, slightly reduces the size of the "gray area", the spanwise grid refinement appears to further delay the onset of resolved turbulence. However, this is accompanied by a somewhat delayed separation, thus indicating a stronger stabilizing effect of the resolved turbulence on the global flow.

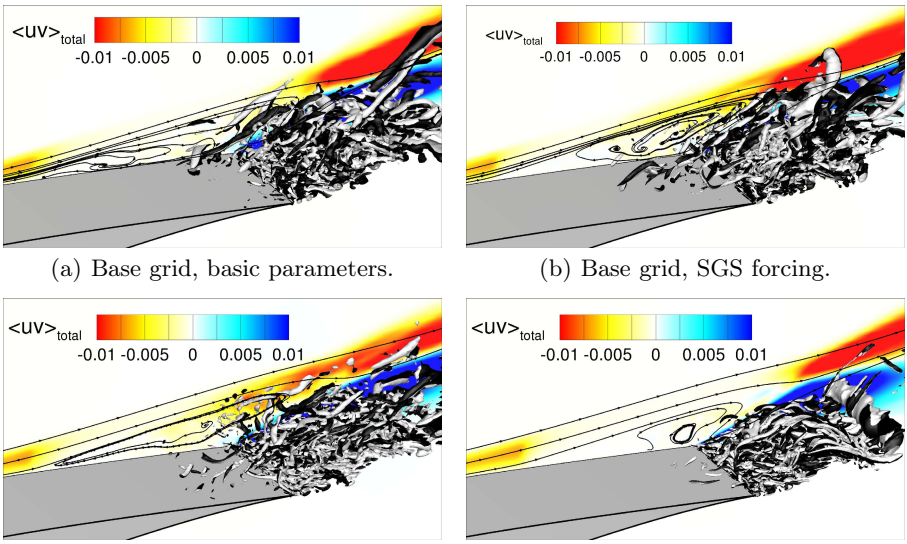

(a) Base grid, basic parameters.

(b) Base grid, SGS forcing.

(c) Grid "$n_z = 1 \rightarrow 64$", $k^{(4)} = 1/160$

(d) Grid "$n_z = 2 \rightarrow 128$".

Fig. 11. Instantaneous Q-criterion ($Q \cdot c^2/U_\infty^2 = 2$) and 2D streamlines as well as total Reynolds shear stress from different SST-ADDES computations of the HGR-01 airfoil at $\alpha = 13°$

The stochastic forcing of the subgrid viscosity in the LES region only slowly enhances the development of vortical structures. For such a shallow separation, the destabilizing effect of SGS forcing is considered much too low to significantly reduce the gap of total shear stress.

Other simulation parameters, such as the physical timestep, were varied as well, but neither showed a considerable impact on the observed behaviour.

5 Conclusions

The zonal RANS-LES method is presented and applied to simulate the flow around an HGR-01 airfoil at high angle of attack. The results are compared with experimental data and pure LES solutions. Averaged pressure and skin-friction coefficients as well as the lift coefficient show good agreement with the LES results. Lift and drag coefficients correspond well with the reference LES computation. The experiments result in the same lift coefficient, but show a slightly smaller trailing-edge separation, and therefore a lower drag coefficient.

The algebraic delayed DES (ADDES) is a non-zonal hybrid method which automatically places the RANS-LES interface near the separation point. While this reduces setup time and computational effort compared to the zonal approach, the underlying SST-RANS model has a stronger impact on the global results: to obtain a significant trailing-edge separation, the angle of attack has to be increased which prevents exact comparison with the zonal method.

Although the ADDES sensors are shown to function properly for the HGR-01 airfoil, the results show a large area of reduced total Reynolds stresses ("gray area") when switching from RANS to LES. This increases the separated region and yields errors in the pressure and skin-friction distributions. Neither variations in the numerical setup, nor a stochastic forcing of the subgrid turbulence have a considerable impact on this behaviour. It is concluded, that more powerful forcing methods, such as the synthetic-turbulence approach used in the zonal RANS-LES method, are required.

This test case is especially challenging for turbulence modeling due to the existence of a laminar separation bubble and a separated flow region at the trailing edge. These unsteady flow phenomena observed in the experiments and the LES simulation are correctly reproduced by the zonal RANS-LES method. The zonal RANS-LES method reduces the computational cost by a factor 4, while approximately maintaining the high accuracy of the pure LES. The RANS limitations for the turbulent boundary layer at the suction side cause the slight deviation of the zonal RANS-LES compared to the pure LES solutions.

References

1. Boris, J.P., Grinstein, F.F., Oran, E.S., Kolbe, R.L.: New insights into large eddy simulation. Fluid Dynam. Res. 10, 199–228 (1992)
2. Celić, A., Hirschel, E.H.: Comparison of eddy-viscosity turbulence models in flows with adverse pressure gradient. AIAA J. 44(10), 2153–2169 (2006)
3. Jarrin, N., Benhamadouche, S., Laurence, D., Prosser, R.: A synthetic-eddy-method for generating inflow conditions for large-eddy simulations. Int. J. Heat Fluid Flow 27, 585–593 (2006)
4. Kok, J., van der Ven, H.: Destabilizing Free Shear Layers in X-LES using a Stochastic Subgrid-Scale Model. Tech. rep., NLR-TP-2009-327 (June 2009)
5. König, D., Meinke, M., Schröder, W.: Embedded LES/RANS boundary in zonal simulations. Journal of Turbulence 11(7), 1–25 (2010), http://dx.doi.org/10.1080/14685241003698159
6. Liou, M.S., Steffen, C.J.: A new flux splitting scheme. J. Comput. Phys. 107, 23–39 (1993)
7. Meinke, M., Schröder, W., Krause, E., Rister, T.: A comparison of second- and sixth-order methods for large-eddy simulations. Comput. Fluids 31, 695–718 (2002)
8. Menter, F.R.: Two-Equation Eddy-Viscosity Turbulence Models for Engineering Applications. AIAA Journal 32(8), 1598–1605 (1994)
9. de Prisco, G., Piomelli, U., Keating, A.: Improved turbulence generation techniques for hybrid RANS/LES calculations. J. Turbul. 9(5), 1–20 (2008)
10. Probst, A., Radespiel, R., Knopp, T.: Detached-Eddy Simulation of Aerodynamic Flows Using a Reynolds-Stress Background Model and Algebraic RANS/LES Sensors. AIAA Paper 2011-3206 (2011)
11. Roidl, B., Meinke, M., Schröder, W.: Zonal RANS-LES computation of transonic airfoil flow. In: 29th AIAA Applied Aerodynamics Conference, AIAA Paper 2011-3974, Honolulu, Hawaii, June 27-30 (2011)
12. Roidl, B., Meinke, M., Schröder, W.: A zonal RANS/LES method for compressible flows. submittet to Comp. Fluids (2011)

13. Schwamborn, D., Gerhold, T., Heinrich, R.: The DLR TAU-Code: Recent Applications in Research and Industry. In: European Conference on Computational Fluid Dynamics (ECCOMAS CFD) P. Wesseling, E. Oñate, J. Périaux (Eds), TU Delft, Niederlande (2006),
http://proceedings.fyper.com/eccomascfd2006/documents/619.pdf
14. Spalart, P.R., Jou, W.H., Strelets, M., Allmaras, S.R.: Comments on the feasibility of les for wings, and on a hybrid RANS/LES approach. In: Advances on DNS/LES, pp. 137–147. Greyden Press, Columbus (1997)
15. Spille-Kohoff, A., Kaltenbach, H.J.: Generation of turbulent inflow data with a prescribed shear-stress profile. In: Third AFSOR Conference on DNS and LES (August 2001)
16. Wokoeck, R., Krimmelbein, N., Ortmans, J., Ciobaca, V., Radespiel, R., Krumbein, A.: RANS Simulations and Experiments on the Stall Behaviour of an Airfoil with Laminar Separation Bubbles. In: 44th AIAA Aerospace Sciences Meeting and Exhibit, AIAA Paper 2006-0244 (2006)
17. Zhang, Q., Schröder, W., Meinke, M.: A zonal RANS/LES method to determine the flow over a high-lift configuration. Comput. Fluids 39, 1241–1253 (2010)